COMMUNICATION

PCCP
www.rsc.org/pccp

Combined EXAFS and STEM-EELS study of the electronic state and location of Mn as promoter in Co-based Fischer–Tropsch catalysts

Fernando Morales,[a] Didier Grandjean,[a] Frank M. F. de Groot,[a] Odile Stephan[b] and Bert M. Weckhuysen*[a]

[a] *Department of Inorganic Chemistry and Catalysis, Utrecht University, Debye Institute, Sorbonnelaan 16, 3584 CA Utrecht, The Netherlands. E-mail: b.m.weckhuysen@chem.uu.nl; Fax: +31302511027; Tel: +31302537400*

[b] *Laboratoire de Physique des Solides, Université Paris-Sud, 91405 Orsay Cedex, France*

Received 6th December 2004, Accepted 19th January 2005
First published as an Advance Article on the web 28th January 2005

STEM-EELS and EXAFS have been used to investigate the location and electronic state of Mn as promoter in TiO_2-supported cobalt Fischer–Tropsch catalysts prepared by two different procedures. It was found that the extent of interaction between Mn and the active Co phase as well as the level of Mn dispersion over the TiO_2 surface largely determine the enhancement of the selectivity in the Fischer–Tropsch synthesis at pressures of 1 bar.

Introduction

An increasing demand for the production of clean liquid fuels in the near future may cause a shift from crude oil to natural gas as the main feedstock used in industry. This will involve the use of Fischer–Tropsch synthesis (FTS) technology, in which linear high-molecular-weight hydrocarbons are synthesized by catalytic hydrogenation of CO using mostly cobalt-based catalysts.[1] These catalysts are often loaded with small amounts of noble metals or metal oxides that enhance significantly their overall catalytic performances. In the present work, we will show that the addition of Mn to a TiO_2-supported Co catalyst has benefits on its FTS selectivity, such as an increase of the C_{5+} yield and a suppression of the undesired methane.[2,3] However, due to the existence of metal-support interactions between the TiO_2 and MnO_x,[4] the addition of Mn does not systematically enhance the catalytic properties. In this regard, the location of MnO_x and its level of segregation seem to play a crucial role. The promotion effect can only be achieved provided a suitable preparation synthesis is used, which leads to a close interaction between MnO_x and the Co active phase in the activated catalyst.

Experimental

Two TiO_2-supported Co-based FTS catalysts were synthesized by the incipient wetness impregnation (IWI) and the homogeneous deposition precipitation (HDP) techniques, using aqueous solutions of $Co(NO_3)_2 \cdot 6H_2O$ (Acros Organics, p.a.) as cobalt precursors and Degussa titania P25 (surface area 45 $m^2\ g^{-1}$, pore volume 0.27 $cm^3\ g^{-1}$) as support material. A more detailed description of the HDP method is addressed in a previous paper.[5] After drying at 110 °C, a portion of each Co/TiO_2 materials was calcined in air at 400 °C for 4 h, leading to two catalysts denoted as I–Co and H–Co, as derived from the first acronym of the preparation technique and the metal contained in the catalyst. A portion of each catalyst was subsequently loaded with Mn (the H–Co after drying and the I–Co after calcination) by IWI using aqueous solutions of $Mn(NO_3)_2 \cdot 4H_2O$ (Merck, p.a.). This step was followed by the same calcination step described above and the obtained catalysts are denoted as I–CoMn and H–CoMn. The crystallized cobalt phase was analyzed by X-ray diffraction (XRD) with an ENRAF-NONIUS XRD system equipped with a curved position-sensitive INEL detector and applying a Co $K\alpha_1$ radiation source ($\lambda = 1.788\ 97$ Å). The size of the formed Co_3O_4 crystallites was estimated using the Scherrer equation (Table 1). The I–CoMn and H–CoMn catalysts were examined by scanning transmission electron microscopy-electron energy loss spectroscopy (STEM-EELS) before and after reduction in H_2 at 350 °C followed by a passivation in CO_2 at 150 °C. The measurements were performed in Orsay (France) with a 100 keV STEM instrument (VG HB 501) equipped with a field emission source and a parallel Gatan 666 spectrometer generating an EELS-spectrum with a 0.5 eV energy resolution and a sub-nanometer spatial resolution within a typical acquisition time of less than one s per pixel.[6] Chemical maps could be generated from the EELS spectra, providing information of the chemical composition in the catalysts along the scanned areas. The Mn local environment was investigated by the extended X-ray absorption fine structure (EXAFS) technique. X-ray absorption data were collected on DUBBLE beamline (ESRF, Grenoble, France), operating under beam conditions of 6 GeV, 200 mA using a Si (111) double-crystal monochromator. The XAS signals of self-supporting wafers were measured at the Mn K edge (before and after *in situ* reduction in H_2 at 350 °C for 2 h) in fluorescence mode using a 9-channel Ge detector. Data reduction and EXAFS refinements of the experimental X-ray absorption spectra were performed using, respectively, the programs EXBROOK and EXCURV98.[7] Phase shifts and backscattering factors were calculated *ab initio* using Hedin–

Table 1 Physicochemical properties of the Co/TiO_2 and Co/Mn/TiO_2 catalysts under study

Catalyst	wt.% Co[a]	wt.% Mn[a]	Co_3O_4 size/nm[b]
I–Co	9.5	0	32
I–CoMn	9.5	0.9	33
H–Co	7.5	0	15
H–CoMn	7.5	2	13

[a] As measured by XRF. [b] Calculated from the line broadening in XRD.

DOI: 10.1039/b418286c

Lundqvist potentials. Refinements were carried out using k^3 weighting in the range 3–10 $Å^{-1}$. The FTS catalytic performances were measured in a plug flow reactor at 1 bar, 220 °C and a H_2/CO ratio of 2 after activation in H_2 at 350 °C for 2 h. The GHSV were adjusted to achieve CO conversions in the range of 3%. The products were separated on-line using a Varian-3200 gas chromatograph equipped with a fused silica column and a flame ionization detector (FID).

Results and discussion

The STEM-EELS measurements provide detailed knowledge of the Mn location and the Co–Mn interactions visualized in chemical maps where Ti, Co and Mn elements are, respectively, coloured in green, red and blue. Fig. 1 shows the EELS images obtained for the freshly calcined catalysts. For details concerning these colour maps we refer to a paper discussing different images of the H–CoMn sample, including a relative quantification of the intensities in the EELS spectra performed in line scans.[8] In the H–CoMn catalyst (images 1A and 1B) it can be clearly seen that Mn is together with the Co_3O_4 leading to purple coloured particles. This suggests the possible formation of a mixed Co/Mn oxide at the surface of the Co_3O_4 particles. In addition, small amounts of MnO_x species are also detected dispersed on the TiO_2 surface though in a minor quantity. The fact that Mn is closely associated with the Co_3O_4 has been shown in a recent work to decrease the amount of Co^0 obtained after reduction at 2 mbar H_2 pressure.[5] In the I–CoMn catalyst a different situation is observed with respect to the MnO_x location, since it is merely covering the TiO_2 surface instead of interacting with the Co_3O_4. In the images 1C and 1D rather large Co_3O_4 particles (>20 nm) are observed, as expected from the XRD results (Table 1), and the MnO_x species are located over the TiO_2 surface. We note that the MnO_x is more clearly seen at the edge of the TiO_2 particles where the Mn signal is better distinguished from the background appearing when a strong Ti signal is present in the EELS spectra.

EXAFS at the Mn K edge complements the STEM-EELS results by providing an insight into the local order around manganese atoms in both Mn-containing catalysts. Fourier transforms of the EXAFS spectra in the two calcined catalysts are presented in Fig. 2. The Fourier transforms show mainly two peaks corresponding, respectively, to Mn–O and Mn–Mn shells. Coordination numbers, bond distances and Debye–Waller factors ($2\sigma^2$) extracted from these two shells are summarized in Table 2, which also includes MnO_2 for comparison. The results indicate that Mn exists in the form of MnO_2 in the I–CoMn catalyst as evidenced from the Mn–O bond distance (1.88 Å), which is almost the same as in the bulk MnO_2. The lower number of neighbours (4.6 to 4.9) in the catalysts compared to 6 in MnO_2 reflects the nanosize and/or the amorphous character of this MnO_2-type phase. In the H–CoMn catalyst the slightly longer Mn–O bond distance (1.902 Å) suggests that the Mn may be forming another compound in addition to MnO_2. Indeed, the EXAFS results together with the STEM-EELS measurements point towards the formation of a solid solution ($Co_{3-x}Mn_xO_4$) wherein Mn^{n+} substitute for Co^{n+} in the spinel structure. It is well known that solid solutions form readily, since both Co and Mn have similar ionic radius and can form stable mixed oxides[10] with Mn–O bond distances linearly increasing from 1.92 to 1.98 Å when x is varying from 0 to 1.3.[11] The combination of these two phases results in a slight increase of the average Mn–O bond distance observed in the H–CoMn catalyst. These findings are supported by the analysis of the XANES region of the spectra, which indicates that the edge position corresponds to a mixture of Mn^{IV} and Mn^{III} in H–CoMn and mainly to Mn^{IV} in I–CoMn. In a recent publication[5] the Mn valence of H–CoMn was measured by soft X-ray absorption and it was found that a mixture of Mn^{II}, Mn^{III} and Mn^{IV} was present at the surface of this catalyst. We attribute the Mn^{II} and Mn^{III} ions to be incorporated in the solid solution and the Mn^{IV} to exist as MnO_2. The existence of some amounts of MnO_2 covering the Co_3O_4 particles cannot be ruled out from these results.

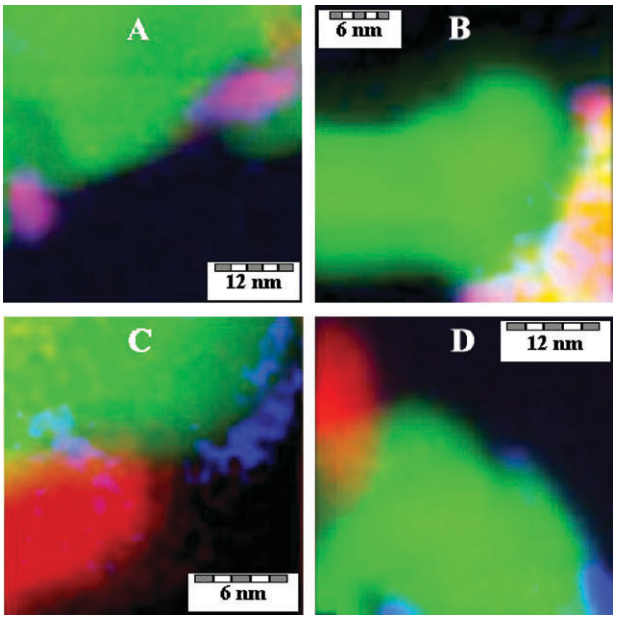

Fig. 1 STEM-EELS images of H–CoMn (A and B) and I–CoMn (C and D) after calcination: Ti (green), Co (red), and Mn (blue).

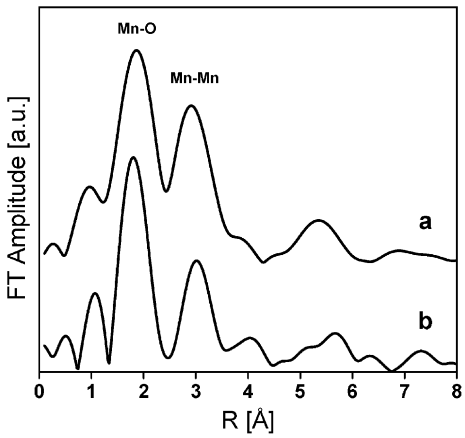

Fig. 2 Fourier transform of the Mn K edge in H–CoMn (a) and I–CoMn (b) after calcination.

The effect of the activation treatment on the Mn location was investigated with STEM-EELS after reduction and passivation. We note that this is an approximation to the real situation after activation, since upon passivation with CO_2 the outer layer of the Co^0 particles is partially reoxidized. It was found that the reduction treatment strongly modified the location and chemical state of Mn. This is shown in Fig. 3, which contains the EELS images of the reduced/passivated catalysts. In the H–CoMn catalyst (images 3A and 3B) no significant changes in the Co particle sizes are found compared to the situation before reduction. On the other hand, the MnO_x species are no longer mixed with the Co, but are partially segregated over the TiO_2 support. This Mn migration was previously investigated in more detail using quantitative XPS analysis.[8] This phenomenon can be explained on the basis that as soon as Co_3O_4 is reduced to Co^0, the MnO_x species are no longer stabilized by the metallic Co and therefore, migrate towards the TiO_2 surface inducing a segregation of Co and Mn phases. Nonetheless, MnO_x clusters are often seen in the vicinity of the Co^0. Their formation is likely favoured by the fact that Co and Mn were associated before reduction. Fig. 3C

Table 2 Results of the EXAFS refinement of the calcined catalysts and the bulk MnO_2 as reference compound

Catalyst	Mn–O/Å	Coord. number	$2\sigma^2$	Mn–Mn/Å	Coord. number	$2\sigma^2$
I–CoMn	1.886	4.6	0.001	2.906	4.5	0.015
H–CoMn	1.906	4.9	0.007	2.887	4.7	0.014
MnO_2[a]	1.885	6	—	2.867	4	—

[a] Crystallographic data of α-MnO_2.[9]

and 3D show the situation in the reduced I–CoMn catalyst. In this case the MnO_x phase exists even more highly dispersed making it difficult to be visualized in the chemical images. A careful examination of the EELS spectra proves that MnO_x homogeneously covers the surface of TiO_2 and even in some regions MnO_x is also found on top of the Co^0 particles (image 3C). Interestingly, the sizes of the Co particles have significantly decreased after reduction, being now in the range of 5–10 nm (Fig. 3C and 3D). Thus, we conclude that the reduction of I–CoMn leads to a segregation of both Co and Mn compounds causing the migration of very small MnO_x particles onto the Co particles, as can be observed in Fig. 3C. The fact that MnO_2 was previously covering the TiO_2 surface as well as the low Mn loading contained in this catalyst (0.9 wt%) seems to induce the formation of such a highly dispersed MnO_x phase uniformly covering the TiO_2 surface as well as some Co^0 particles. These findings resemble the studies of strong metal support interaction (SMSI) in supported noble metals,[12,13] which showed that reduction of TiO_2-supported noble metals at high temperatures occasionally results in the migration of partly reduced TiO_x suboxide phases onto the metal particles leading to a partial blockage of the metal surface and consequently to a decrease in the chemisorption capacity of the metals.

In Fig. 4 the Fourier transforms of the reduced catalysts clearly show that a loss in the long range order around Mn has occurred upon reduction in both materials since the contribution of further shells is no longer visible. This effect is even more pronounced in the I–CoMn catalyst, in which only the first shell corresponding to the Mn–O bond is observed. This is a clear indication of the high level of dispersion of the MnO_x phase in these materials that deflects from the more ordered phases. In H–CoMn the second shell corresponding to the Mn–Mn bond is still present but with a very low intensity, pointing towards the existence of larger MnO_x particles in addition to the highly dispersed phase (Fig. 4). A careful comparison of the edge position in the XANES region of the spectra of both reduced catalysts as well as in the MnO and Mn_2O_3 reference compounds reveals that all the manganese is entirely in a divalent state (Mn^{II}). As an example, the XANES spectra of the H–CoMn catalyst before and after the reduction treatment are shown in Fig. 5, the edge position being indicative of a Mn^{III}/Mn^{IV} mixed valence and a Mn^{II} valence before and reduction, respectively. However, the Mn–O distances differ significantly from the typical distance in bulk MnO (2.22 Å). This is shown in Table 3, which summarizes the parameters obtained upon fitting the first two shells in both reduced catalysts and in a MnO and Ti_2MnO_4 reference compounds. A Ti_2MnO_4-type amorphous phase seems to form during reduction in the I–CoMn catalyst, as evidenced from the Mn–O distance, which is *ca.* 2.04 Å in both materials. Moreover, the oxygen coordination number obtained for the first shell in I–CoMn (4.3) is very close to the 4-fold coordination as in the Ti_2MnO_4 compound, in which the Mn^{2+} ions are coordinated by four oxygens in a spinel structure. The slight greater oxygen coordination number may be due to the small MnO particles found on top of the Co. Hence, most of the Mn^{II} ions appear to exist highly dispersed in the proximity of

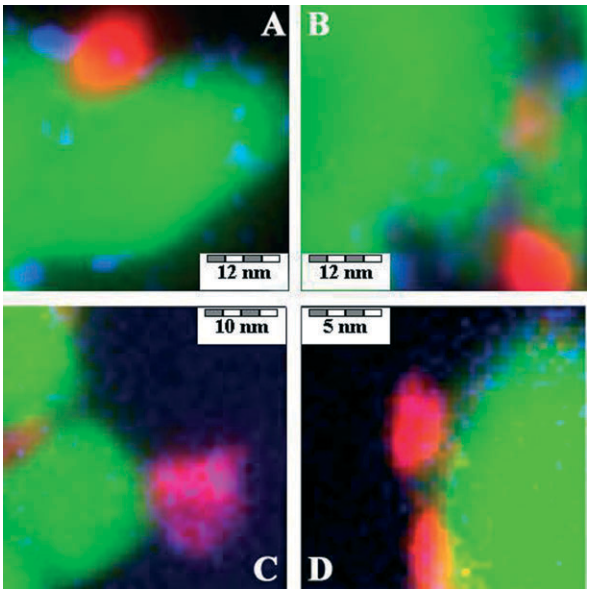

Fig. 3 STEM-EELS images of H–CoMn (A and B) and I–CoMn (C and D) after reduction in H_2 at 350 °C and passivation at 150 °C in CO_2.

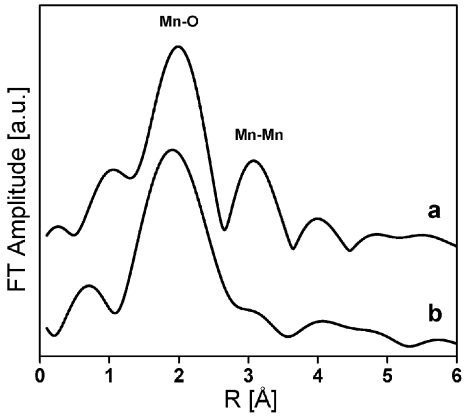

Fig. 4 Fourier transform of H–CoMn (a) and I–CoMn (b) after reduction in H_2 at 350 °C for 2 h.

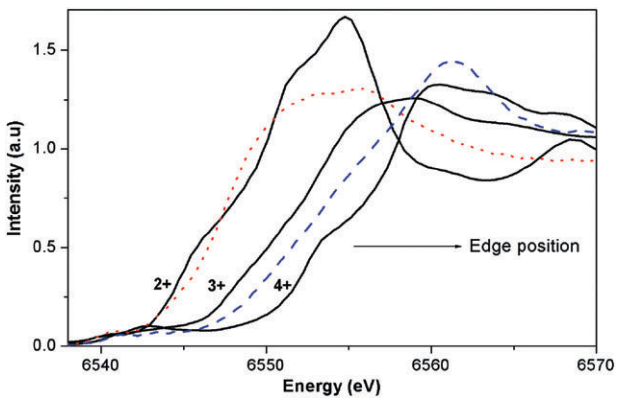

Fig. 5 XANES spectra of the reference oxides, MnO (2+), Mn_2O_3 (3+) and MnO_2 (4+), and the H–CoMn catalyst after calcination (dashed) and after reduction (dotted).

Table 3 Results of the EXAFS refinement of the reduced catalysts and two reference compounds

Catalyst	Mn–O/Å	Coord. number	$2\sigma^2$	Mn–Mn/Å	Coord. number	$2\sigma^2$
I–CoMn	2.039	4.3	0.030	—	—	—
H–CoMn	2.072	5.2	0.033	3.039	1.0	0.010
MnO[a]	2.220	6	—	3.140	12	—
Ti_2MnO_4[a]	2.041	4	—	3.724	4	—

[a] Crystallographic data.[9]

the Lewis acid sites (Ti^{4+}) throughout the surface of TiO_2 and thereby forming a mixed Mn/Ti surface compound. The surface of titania contains numerous Lewis acid sites classified as α, β and γ in decreasing strength.[14,15] These Lewis acid sites may play a role in stabilizing the MnO_x species at the surface during reduction. The formation of titanate compounds is induced by the strong metal-support interactions (SMSI) existing between MnO_x and TiO_2, which causes the incorporation of Mn^{2+} ions into the TiO_2 lattice upon reduction[4] resulting in the formation of a Ti_2MnO_4-type amorphous phase at the outer layer of the TiO_2 surface. In the H–CoMn catalyst the presence of a weak Mn–Mn second shell combined with the slightly longer Mn–O bond distance (2.07 Å) and a higher coordination number (5.2), suggest that the formation of titanates occurs to a lower extent. Thus, in addition to the Ti_2MnO_4-type phase, the H–CoMn catalyst also contains some larger MnO particles. These results obtained from EXAFS are in line with the EELS images discussed above, wherein well-distinguished MnO particles are clearly visible in the vicinity of the Co.

Table 4 summarizes the FTS catalytic results obtained after stabilization of the activities (*ca.* 40 h reaction). In the H–CoMn catalyst a clear promotion effect is achieved with both an enhanced selectivity and activity. The MnO causes a suppression of the CH_4 production (7%), an increase of the C_{5+} yield (6%), and a very slight increase of the Co-time yield. In addition, the chain growth probability (α) increases from 0.54 to 0.58. These changes in the selectivity of H–CoMn were discussed in a previous paper.[8] On the other hand, the catalytic properties of the I–CoMn catalyst are not enhanced by the presence of Mn. Instead, the Mn moderately reduces the Co-time yield and the C_{5+} selectivity. Furthermore, it is clear that the I–Co and I–CoMn catalysts display superior performances to produce high hydrocarbons compared to the H–Co and H–CoMn catalysts. This is related to the active Co phase formed after reduction, which turns out to be more selective towards high hydrocarbons in the catalysts prepared by IWI. Nevertheless, with regard to the Mn promotion, which is the aim of this work, it can be concluded that the state and location of the Mn species largely determine the effectiveness of the promotion. Fig. 6 summarizes schematically the state and location of Mn in both catalysts before and after the reduction. The formation of Ti_2MnO_4 compounds occurs to a great extent in the I–CoMn catalysts upon reduction and these titanates are spectator species during the FTS reaction. In the I–CoMn catalyst the catalytic performances are not enhanced but, on the contrary, poisoned by the presence of very small MnO particles blocking a fraction of the Co^0 active sites. In the H–CoMn catalyst the existence of MnO particles not strongly interacting with the TiO_2 and located in the proximity of the Co^0 sites leads to a promotion effect. Hence, we can conclude that these MnO-type species are needed in order to achieve promotion in FTS. Further investigations are needed to establish how the MnO modifies the reaction mechanism and hence, the catalytic performances of these FTS catalysts.

Table 4 Catalytic properties of the catalysts after 40 h FTS reaction

Catalyst	Co-time yield[a]	Wt% CH_4	Wt% C_{5+}	α value[b]
I–Co	1.6	21	48	0.69
I–CoMn	1.2	21	45	0.66
H–Co	2.3	32	28	0.54
H–CoMn	2.5	25	34	0.58

[a] 10^{-5} mol CO (g Co)$^{-1}$ s^{-1}. [b] As calculated from the slope between C_3 and C_7 in the ASF distribution plot, according to the equation $\log W_n/n = \log(\ln^2 \alpha) + n \log \alpha$, where W_n is the weight fraction of the products with n carbon number.

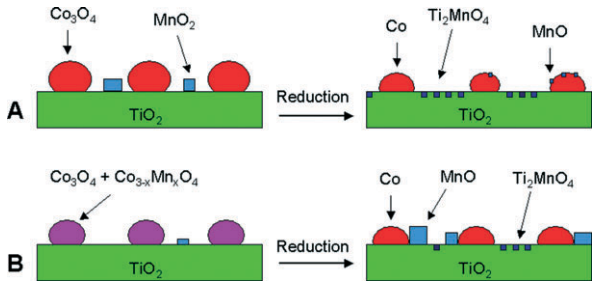

Fig. 6 Schematic representation of the I–CoMn (A) and H–CoMn (B) catalysts before and after the reduction treatment.

Conclusions

The combination of EXAFS and STEM-EELS is a very powerful tool for investigating highly dispersed multiphase materials. The location of MnO_x in Co/TiO_2 FTS catalysts is strongly affected by the preparation procedure and as a consequence determines the effectiveness of Mn as a promoter. The preparation procedure carried out to synthesize the I–CoMn catalyst leads to the formation of large Co_3O_4 particles and a MnO_2 phase located mainly on the TiO_2 support. After reduction, a Ti_2MnO_4-type phase is formed upon migration of Mn^{n+} ions into the TiO_2 structure. This highly dispersed Ti_2MnO_4-type phase does not enhance the catalytic performances, but remains as a spectator species. Furthermore, some small MnO particles located on top of the Co partially block some active sites leading to a decrease in the Co-time yield. On the other hand, the preparation procedure used to synthesize the H–CoMn catalyst results in the association of Co and Mn oxides and the formation of a $Co_{3-x}Mn_xO_4$ solid solution. This favors the formation of MnO particles in the proximity of Co^0 upon reduction, which directly play a role under FTS condition. Hence, the presence of this MnO phase in the vicinity of the Co^0 particles enhances the selectivity in the FTS by increasing the percentage of higher hydrocarbons. These findings represent a breakthrough in understanding the MnO promotion effect in the FTS.

Acknowledgements

The authors gratefully acknowledge financial support from Shell Global Solutions, the Universite Paris-Sud (Orsay, Paris) for the STEM-EELS measurements, and the E.S.R.F synchrotron (Grenoble) for the XAS measurements. We thank S. Nikitenko for his assistance and advise during EXAFS

experiments. The work also benefited from fruitful discussions with H. Oosterbeek, H. Kuipers and C. Mesters of Shell Global Solutions.

References

1 E. Iglesia, *Appl. Catal., A*, 1997, **161**, 59.
2 M. van der Riet, R. G. Copperthwaite and G. J. Hutchings, *J. Chem. Soc., Faraday Trans 1*, 1987, **83**, 2963.
3 G. J. Hutchings, R. G. Copperthwaite and M. van der Riet, *Top. Catal.*, 1995, **2**, 163.
4 M. Kantcheva, M. U. Kucukkal and S. Suzer, *J. Catal.*, 2000, **190**, 144.
5 F. Morales, F. M. F. de Groot, P. Glatzel, E. Kleimenov, H. Bluhm, M. Havecker, A. Knop-Gericke and B. M. Weckhuysen, *J. Phys. Chem. B*, 2004, **108**, 16201.
6 O. Stephan, A. Gloter, D. Imhoff, M. Kociak, K. Suenaga, M. Tence and C. Colliex, *Surf. Rev. Lett.*, 2000, **7**, 475.
7 N. Binstead, J. W. Campbell, S. J. Gurman and P. C. Stephenson, *EXAFS Analysis Programs*, 1991, Daresbury Laboratory, Warrington.
8 F. Morales, F. M. F. de Groot, O. L. J. Gijzeman, A. Mens, O. Stephan and B. M. Weckhuysen, *J. Catal.*, 2005, (in press).
9 D. A. Fletcher, R. F. McMeeting and D. Parkin, *J. Chem. Inf. Comput. Sci.*, 1996, **36**, 746.
10 E. Vila, R. M. Rojas, J. L. Martin de Vidales and O. G. Martinez, *J. Mater. Chem.*, 1994, **4**, 1635.
11 J. L. Martin de Vidales, E. Vila, R. Rojas and O. Garcia-Martinez, *Chem. Mater.*, 1995, **7**, 1716.
12 M. A. Vannice, *J. Catal.*, 1982, **74**, 199.
13 C. L. Haller and D. E. Resasco, *Adv. Catal.*, 1989, **36**, 173.
14 K. Hdjiivanov, D. Klissurski and A. Davydov, *J. Chem. Soc., Faraday Trans.*, 1998, **1**, 84.
15 K. Hadjiivanov, J. Lamotte and J. Lavalley, *Langmuir*, 1997, **13**, 33.

